OXFORD Toxicology Research

Toxicology Research, 2021, **10**, 51–59

doi: 10.1093/toxres/tfaa092
Advance Access Publication Date: 5 January 2021
Paper

PAPER

L-carnitine suppresses cisplatin-induced renal injury in rats: impact on cytoskeleton proteins expression

Osama Fouad Ahmed Ebrahim,[1] Ola Elsayed Nafea,[2,3,*] Walaa Samy[4] and Lamiaa Mohamed Shawky[5]

[1]Department of Anatomy, Faculty of Medicine, Benha University, Benha 13518, Egypt, [2]Department of Forensic Medicine and Clinical Toxicology, Faculty of Medicine, Zagazig University, Zagazig 44519, Egypt, [3]Department of Clinical Pharmacy, Collage of Pharmacy, Taif University, Taif 11099, Saudi Arabia, [4]Department of Medical Biochemistry, Faculty of Medicine, Zagazig University, Zagazig 44519, Egypt and [5]Department of Histology and Cell Biology, Faculty of Medicine, Benha University, Benha 13518, Egypt

*Correspondence address. Faculty of Medicine, Department of Forensic Medicine and Clinical Toxicology, Zagazig University, Zagazig 44519, Egypt. Tel: +201026269962; E-mail: olanafea@zu.edu.eg or olaenafea@gmail.com

Abstract

We designed this work to examine the curative role of L-carnitine (LCAR) in a rat model of cisplatin (CDDP)-induced kidney injury. We induced kidney injury in rats by a single intraperitoneal injection of 5 mg/kg of CDDP. Fifteen days post injection, rats were orally supplemented with 354 mg/kg of LCAR for another 15 days. Kidney tissues were subjected to histo-biochemical analysis along with mRNA gene expression quantification for cytoskeleton proteins encoding genes (vimentin, nestin, and connexin 43) by real-time reverse transcription polymerase chain reaction. LCAR reversed CDDP-induced renal structural and functional impairments. LCAR significantly declined serum urea and creatinine concentrations, restored oxidant/antioxidant balance, reversed inflammation, and antagonized caspase 3-mediated apoptotic cell death in renal tissues. Moreover, LCAR effectively down-regulated cytoskeleton proteins mRNA levels, reflecting amelioration of CDDP-provoked podocyte injury. We concluded that LCAR has a favorable therapeutic utility against CDDP-induced kidney injury.

Key words: cisplatin, gap junction proteins, intermediate filaments, L-carnitine, podocyte

Introduction

Cisplatin, cis-diammine dichloridoplatinum II (CDDP) is an effective antineoplastic agent. Currently, the World Health Organization listed CDDP as one of the essential medicines. CDDP is one of the most commonly utilized chemotherapeutic agents for hematologic and solid tumor cancers [1, 2]. CDDP exerts its cytotoxic effect through crosslinking purine bases within the DNA strands; causing DNA damage in malignant cells, blocking cell division with resultant apoptotic cell death [3]. In this way, other non-targeted organ toxicities can develop. Renal dysfunction is one of the most encountered complications of CDDP that limits its clinical applications [4–6].

Acute kidney injury (AKI) is the most serious and frequently reported side effect of CDDP. Approximately 20–30% of CDDP-received patients developed AKI [7, 8]. The nephrotoxicity of CDDP is cumulative and dose related. Patients who develop AKI are more likely to develop chronic kidney injury and an increased risk of mortality [4, 9].

Several postulated mechanisms of CDDP-induced kidney injury include mitochondrial dysfunction, DNA damage, oxidative stress, and inflammatory response [9–12].

Received: 22 September 2020; **Revised:** 26 October 2020; **Accepted:** 3 November 2020

Carnitine is an essential dietary nutrient that has a wide range of biological functions. Carnitine exists in two forms (D-carnitine and L-carnitine). L-carnitine (LCAR) is the biologically active form, while D-carnitine is toxic. LCAR has an imperative role in energy metabolism because it acts as a carrier for activated long-chain fatty acids from the cytosol to the mitochondrial matrix, where they are broken down via β-oxidation [13]. LCAR is synthesized in the human body from L-lysine and L-methionine amino acids, mainly in the kidney and the liver as well as it can be obtained exogenously from dietary sources [14].

In 1986, The Food and Drug Administration approved LCAR as an orphan drug for primary LCAR-deficiency treatment. Moreover, the drug can be exploited in conditions associated with secondary LCAR deficiency, e.g. renal disorders [15].

Intermediate filaments (IFs) are one of the eukaryotic cytoskeleton proteins that are involved in the cell mechanical properties. IFs are characterized by distinctive extensibility and striking resilience that allow them to support cells against exterior and interior forces [16, 17]. Currently, IFs are involved in many vital biological pathways [18].

Vimentin (Vim) is the most abundant and the studied type III IFs protein [19]. Nestin (Nes) is another IFs principally expressed in neural stem cells. Nes is expressed transiently in the glomerular podocytes and is imperative for the maintenance of the podocyte foot process [20].

Gap junction proteins (connexins/Cxs) are key players in the cellular connection, also they are critical in numerous vital modulatory processes in the kidney, e.g. the renin-angiotensin system, tubule-glomerular feedback, and salt and water retention [21, 22]. Connexin 43 (Cx43) is found in the renal tubules and vasculatures. Furthermore, Cx43 is mostly found in glomerular podocytes [23].

The underpinning molecular mechanisms of the 'sick' podocyte have attracted escalating interest, which is pivotal in keeping the integrity of the glomerular filtration barrier. The podocyte has a distinctive cytoskeleton that is dynamically controlled by constant alterations in contractility and motility. The discontinuity of integrity of the cytoskeleton proteins may cause podocytopathy with the subsequent decline in kidney function [24, 25].

We hypothesized that LCAR would reverse CDDP-induced kidney injury. Accordingly, we conducted this study to examine the curative role of LCAR supplementation in a rat model of CDDP-induced kidney injury as well as the underlying mechanisms, focusing on the cytoskeleton proteins encoding genes: Vim, Nes, and Cx43.

Materials and Methods

Materials

We purchased CDDP (Cisplatin® a vial contains 1 mg/ml of CDDP, Mylan institutional LLC, Rockford, IL, USA), LCAR (a liquid-formulation of 300 mg/ml, MEPACO-MEDIFOOD Company, Sharkia, Egypt).

Animals

The study included 40 adult male albino rats weighing 280–300 g, which were obtained from the Breeding Unit of the Egyptian Organization for Biological Products and Vaccines, VACSERA, Cairo, Egypt. The animals were housed in plastic cages with 12-h light and dark cycles, and allowed free access to food and water. For acclimation purposes, the rats were handled manually for 1 week before the experiment to allow biological stabilization. All animals received humane care in compliance with the Animal Care Guidelines of the National Institutes of Health and the Department of Anatomy, Benha Faculty of Medicine approved the design of the experiment.

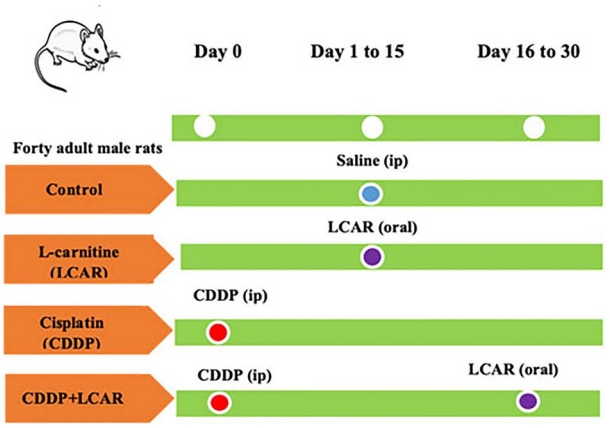

Figure 1: Study design.

Experimental design. We randomly assigned animals into four groups of 10 rats each: control, LCAR, CDDP, and (CDDP + LCAR) groups (Fig. 1).

Group I (normal control): Received saline (1 ml daily), intraperitoneal injection (ip).

Group II (LCAR): Supplemented with LCAR in a dose of 354 mg/kg body weight, orally, once daily for 15 successive days.

Group III (CDDP): Treated with CDDP in a single dose of 5 mg/kg, ip.

Group IV (CDDP + LCAR): Treated with CDDP in a single dose of 5 mg/kg body weight, ip; then 15 days later, these rats were supplemented with LCAR in a dose of 354 mg/kg body weight, orally, once daily for another 15 successive days.

Previous animal studies indicated that a single intraperitoneal injection of 5 mg/kg CDDP can induce acute kidney failure [26–28]. Clinical benefits were reported following daily oral administration of LCAR (4–6 g) in cancer patients, in terms of safety, effectiveness and alleviation of chemotherapy-related complications [29–31]. The selected dose of LCAR (354 mg/kg/day) is parallel to the human dosing regimen of 4 g/day based on body surface area conversion [animal dose (mg/kg) = human equivalent dose (mg/kg) × 6.2], supposing that an adult person weighs 70 kg [32, 33]. At the end of the treatment protocol, rats were anesthetized intraperitoneally with pentobarbital (60 mg/kg) [34]. Blood was collected from the ophthalmic plexus for the separation of serum. Serum samples were obtained by centrifugation of blood at 2683*g* for 20 min and stored at −20°C. The kidneys were excised immediately for histological and biochemical analyses.

Histological and immunohistochemical studies

The kidneys were dissected and fixed in 10% formal saline for later processing of paraffin sections. According to previously described protocols, approximately 5-µm renal sections were cut and subjected to hematoxylin and eosin [35], Mallory's trichrome stain [36] and immunohistochemical staining using the peroxidase-labeled streptavidin–biotin method for detection of transforming growth factor-β (TGF-β1) antibody [37]. The primary antibody used was mouse monoclonal antibody (Lab

Vision Corporation, Fremont, CA, USA). It was ready for the staining of formalin-fixed and paraffin-embedded tissues. The sections were incubated with the primary antibody diluted to a concentration of 1:100 in PBS for 1 h, followed by a reaction with a biotinylated secondary antibody. After conjugation with streptavidin–biotin–peroxidase complex, 3,3-diaminobenzidine was used as a chromogen, and hematoxylin solution was used as a counterstain. The reaction gives brownish cytoplasmic discoloration. All tissue specimens were examined by Olympus Light Microscope. Image acquisition was performed with a digital microscope camera (Leica Qwin 500, Leica, England) computer system.

For electron microscopy, according to Woods and Stirling [38], small renal cortex specimens (1 mm^3) were fixed in 2.5–3% glutaraldehyde solution in 0.1 M phosphate buffer, pH 7.4 at 4°C for 2 h, followed by post-fixation in 1% osmium tetroxide at 4°C for 30 min, then dehydrated in serial dilutions of ethanol and finally embedded in epoxy resin (Epoxy Embedding Medium Kit; Sigma). Ultra-thin sections (70 nm) were cut using Leica Ultramicrotome, stained with uranyl acetate and lead citrate to be examined by JEM-2100 transmission electron microscope (TEM) (JEOL, Tokyo, Japan), at the Electron Microscope Unit, at Faculty of Agriculture, Mansoura University, Mansoura, Egypt.

Morphometric study

We used the image analysis computer system (Leica Qwin 500 MC, Leica, England), at the Faculty of Science, Tanta University, Tanta, Egypt. The image analyzer was first calibrated automatically to convert the measurement units (pixels) produced by the image analyzer program into actual micrometer units. It was used to measure the area percent of collagen fibers deposition in Mallory's Trichrome stained sections and the area percent of TGF-β1 immunoreaction, in all experimental groups. These measurements were performed in seven different, non-overlapping fields at a magnification of 400 per slide in all groups. The coloration of the TGF-β1 immunostained and trichrome-stained areas was covered automatically by a blue mask (binary image). The area of this binary image was then calculated, which reflected the areas of marked TGF-β1 immunoreactivity and excess collagen deposition.

Biochemical analysis

Assessment of kidney function biomarkers. Serum concentrations of urea and creatinine were measured colorimetrically using the commercially available assay kits (Biodiagnostic Company, Dokki, Giza, Egypt).

Measurement of renal inflammatory biomarkers [tumor necrosis factor-alpha (TNF-α) and interleukin-10 (IL-10)] and oxidant/antioxidant biomarkers [malondialdehyde (MDA) level and catalase (CAT) activity].

Renal levels of TNF-α and IL-10 were assessed by the commercially available assay ELISA kits (RayBiotech, USA). Both renal MDA level and CAT activity were measured colorimetrically by the commercially available assay kits (Biodiagnostic Company, Dokki, Giza, Egypt). TNF-α and IL-10 were normalized per 100 µg protein sample.

Assessment of renal caspase-3 activity. Renal activity of caspase-3 was assayed by the commercially available assay ELISA kits (Rat Casp-3, My Biosource, USA).

Gene expression analysis

Sample preparation and RNA isolation. Total RNA was isolated from the kidney tissues according to the RNA isolation kit (Gentra, Minneapolis, MN 55441, USA) following the manufacturer's protocol. The purity and integrity of total RNA were monitored by "absorbance of ultraviolet spectrophotometer" at 260/280 nm.

Reverse transcription and cDNA synthesis. For the synthesis of complementary DNA (cDNA), the extracted RNA was reverse transcribed by QuantiTect SYBR Green RT–PCR kit (Qiagen; Catalog No. 204243) as recommended by the manufacturer.

Real-time polymerase chain reaction for mRNA gene expression. Expression levels of mRNA were determined by real-time polymerase chain reaction using Step One TM System (Applied Biosystems). Glyceraldehyde-3-phosphate dehydrogenase (GAPDH) used as an internal control. Primer sequences were reported in Table 1. Polymerase chain reaction (PCR) was performed in 25 µl containing 12.5 µl QuantiFast SYBR Green (Cat. No. 204141) PCR Master Mix, 1 mM of each primer Invitrogen, USA and 2 µl cDNA. The amplification conditions include initial activation 95°C/15 s followed by 40 cycles of denaturation 94°C/15 s, annealing at 60°C/15 s, and elongation at 72°C/15 s. The relative expression was calculated from the $2^{-\Delta\Delta CT}$ formula. All kits were supplied by QIAGEN (Valencia, CA).

Statistical analysis

Continuous variables are presented as the mean ± standard deviation (SD). We checked the normality of the continuous variables by Shapiro–Wilk test while the equality of variance by Bartlett's test. We used a one-way analysis of variance (ANOVA) or Welch's ANOVA test according to equality of variance to detect statistical differences between groups. Furthermore, *post-hoc* tests (Tukey test if equal variances are assumed; Tamhane's T2 test if equal variances are not assumed) were performed for multiple comparisons between groups. The differences were considered significant at $P < 0.05$. All statistical comparisons were two-tailed. All statistical analyses were calculated using Graphpad Prism, Version 8.0 Software (GraphPad Software, San Diego, CA, USA).

Results

LCAR supplementation mitigated renal histopathological lesions induced by CDDP administration in rats

Examination of H&E stained sections from the control and LCAR-supplemented rats is alike and reveals the normal renal histoarchitecture. The renal corpuscles appeared with normal capillary tuft surrounded by Bowman's capsule with patent Bowman's (filtration) space in-between. The proximal convoluted tubules (PCTs) were lined by cubical cells with acidophilic granular cytoplasm, rounded vesicular nuclei and intact apical brush border. The distal convoluted tubules (DCTs) showed wider lumina and lined with low cubical cells with rounded nuclei (Fig. 1a). CDDP group revealed marked ultrastructural alterations. The tubular lining cells appeared swollen with almost loss of the patency of some renal tubules. Necrotic epithelial cellular debris were seen inside the lumina of some renal tubules. Many tubular cells showed vacuolated cytoplasm with loss of the apical brush border, others showed pyknotic nuclei. The renal interstitium showed mononuclear cellular infiltrates and mild

Table 1: Oligonucleotide primer sequences used in the quantitative PCR measurement for Vim, Nes, Cx43, and GAPDH

Gene	Primers sequences	GenBank® accession number
Vim	Forward: 5′-TTCTCTGGCACGTCTTGACC-3′ Reverse:5′-TCCTGTAGGTGGCGATCTCA-3′	NM_031140.1
Nes	Forward: 5′-TGATGGCTTGAGAGGTGCTG-3′ Reverse:5′-AGGATCTCACCTCCCTTGCT-3′	NM_012987.2
Cx43	Forward: 5′-GGATTTTTGTGGTGTGGGCC-3′ Reverse:5′-ACTGTTGAAACCTCCCTCGC-3′	NM_012567.2
GAPDH	Forward: 5′-TTCACCACCATGGAGAAGGC-3′ Reverse:5′-CCCAGGATGCCCTTTAGTGG-3′	NM_017008.4

Abbreviations: Vim, Vimentin; Nes, Nestin; Cx43, Connexin 43; GAPDH, Glyceraldehyde-3-phosphate dehydrogenase

congestion of some blood capillaries (Fig. 1b and c). LCAR supplementation alleviated most of the histopathological lesions provoked by CDDP treatment. Almost complete restoration of the renal microstructure was evident. The renal corpuscles showed normal glomeruli with normal filtration spaces. The/renal tubules appeared normal with preserved brush borders. Only minimal peritubular vascular congestion was seen (Fig. 2d and e).

LCAR supplementation decreased renal TGF-β1 immunoexpression following CDDP administration in rats

TGF-β1 immunostained sections are quite similar and showed a faint TGF-β1 cytoplasmic immunoexpression in glomeruli and renal tubules in the control and LCAR-supplemented groups (Fig. 3a). The CDDP group showed a diffuse positive TGF-β1 cytoplasmic immunoexpression in the glomeruli and renal tubules (Fig. 3b). While LCAR supplementation elicited a negative TGF-β1 immunoexpression in renal tubules and a slightly positive TGF-β1 reaction in scarce glomeruli (Fig. 3c). Morphometric analysis of renal tissues showed that mean TGF-β1 immunoexpression significantly increased in CDDP group than control, LCAR and CDDP + LCAR groups ($P < 0.001$, each) (Fig. 5a).

LCAR supplementation diminished renal collagen fiber deposition following CDDP administration in rats

Mallory's trichrome stained sections of the control group and LCAR-supplemented group demonstrated normally distributed collagen fibers around glomeruli and renal tubules within the renal cortex (Fig. 3d). However, the CDDP group displayed a marked collagen fibers deposition around the glomeruli and in renal interstitium (Fig. 2e). In CDDP + LCAR-treated rats, collagen fiber deposition was minimal around glomeruli and renal tubules (Fig. 2f). Morphometric analysis of renal tissues showed that mean area percent of collagen fiber disposition highly significantly increased in CDDP group than control, LCAR, and CDDP + LCAR groups ($P < 0.001$, each) (Fig. 5a).

LCAR supplementation reversed renal ultrastructural lesions induced by CDDP administration in rats

Using TEM, the renal tissue did not reveal substantial differences among rats in the control and LCAR-supplemented groups and it was parallel to the well-known normal ultrastructural pattern of PCTs and DCTs as well as renal glomeruli. PCTs lining cells appeared with euchromatic nuclei, closely packed long apical microvilli, and elongated mitochondria (Fig. 4a). DCTs lining cells were low cubical cells, with euchromatic nuclei, few apical short microvilli basal membrane infoldings alternating with elongated mitochondria (Fig. 4d). Within the renal glomeruli, podocytes were irregular cells; each with a cell body and thick multiple primary processes. Each primary process gave rise to several secondary thin processes that ended in a pedicle-like expansion implanting on a thin glomerular basement membrane (Fig. 4g). In the CDDP group, the TEM examination displayed marked ultrastructural changes in PCTs and DCTs as well as renal glomeruli. PCTs lining cells showed degenerative changes in the form of a damaged apical membrane with extrusion of cellular organelles into the lumen, a partial loss of the apical microvilli, swollen mitochondria, and absent basal infoldings. In addition, cytoplasmic vacuoles and marked rarefaction (clear areas) of cytoplasm could be observed (Fig. 4b). DCTs lining cells showed interrupted basal infoldings, swollen pleomorphic mitochondria with detached dispersed cristae (cristolysis). The nucleus had less electron density. Cytoplasm appeared markedly rarefied with less electron density and many cytoplasmic vacuoles (Fig. 4e). The glomerular basement membrane showed focal irregular thickening. The podocytes showed an irregular nucleus with peripherally condensed chromatin. The secondary processes appeared thickened, closely related, and fused with obliteration of the filtration slits (Fig. 4h). LCAR supplementation reversed the remarkable ultrastructural lesions elicited by CDDP treatment. The renal tubular lining cells appeared with normal euchromatic nuclei, preserved apical microvilli, normally shaped and normally oriented mitochondria (Fig. 4c and f). The normal ultrastructure of the renal corpuscle is restored. The glomerular basement membrane retained its normal thickness. The normal shape and thickness of primary and secondary processes of podocytes were restored with preserved filtration slits (Fig. 4i).

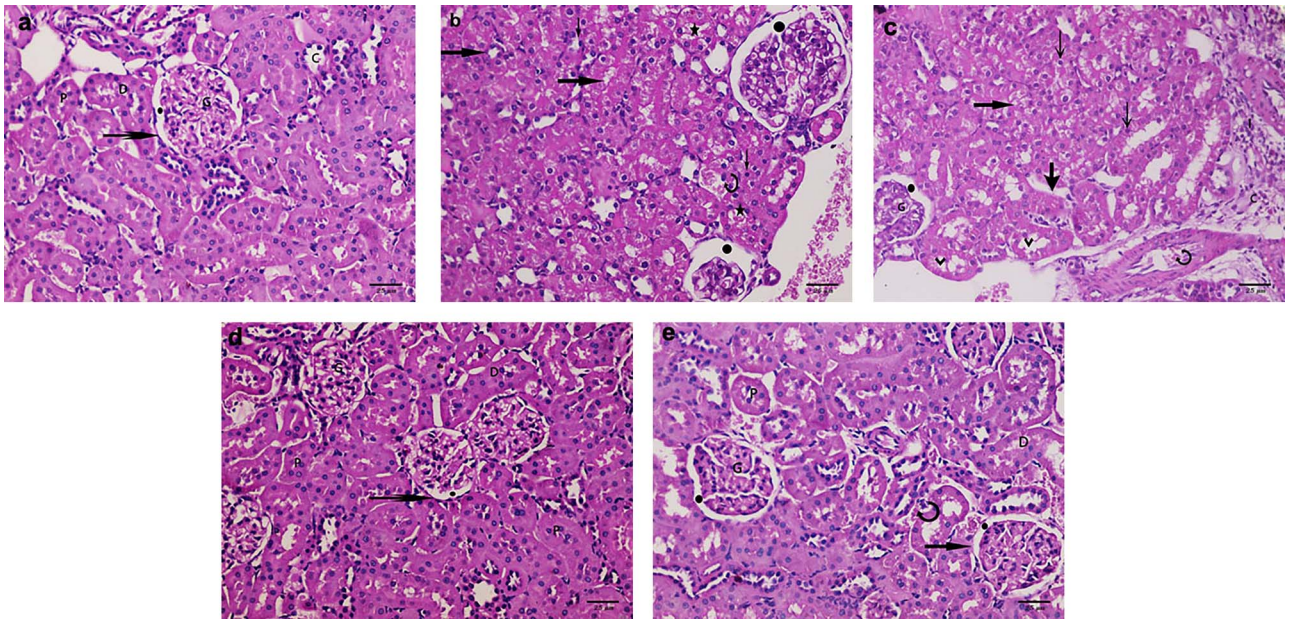

Figure 2: (**a**) The renal cortex of a control rat showing normal glomerular structure (G), surrounded by Bowman's capsule (arrow), filtration space (a black circle). Proximal convoluted tubules (P) have intact apical brush borders. The distal convoluted tubules (D) and collecting ducts (C) show normal morphology. (**b**, **c**) The renal cortex of a rat from the CDDP group showing the renal tubules (thick arrows) with degenerative changes in the form of swollen tubular cells with vacuolated cytoplasm and narrowed lumina. Some renal tubules show pyknotic nuclei (thin arrows) and desquamated necrotic cellular debris inside the lumina (stars), others show destroyed apical membrane with loss of their nuclei (arrowhead). Renal glomeruli (G) appear atrophic with disorganized structural arrangement and widened filtration space (black circles). A crowd of inflammatory cells (I) is evident in the connective tissue (C) interstitium. Congested blood capillaries (curved arrow) are seen. (**d**, **e**) The renal cortex of a rat from CDDP + LCAR group showing approximately normal histoarchitecture of the renal parenchyma with normal glomerular structure (G), Bowman's capsule (arrows), and filtration space (black circles). Proximal convoluted tubules (P) with preserved brush border with mild peritubular hemorrhage (curved arrow) can be seen. Distal convoluted tubules (D) show normal structure. (H&E 400), scale bar = 25 µm.

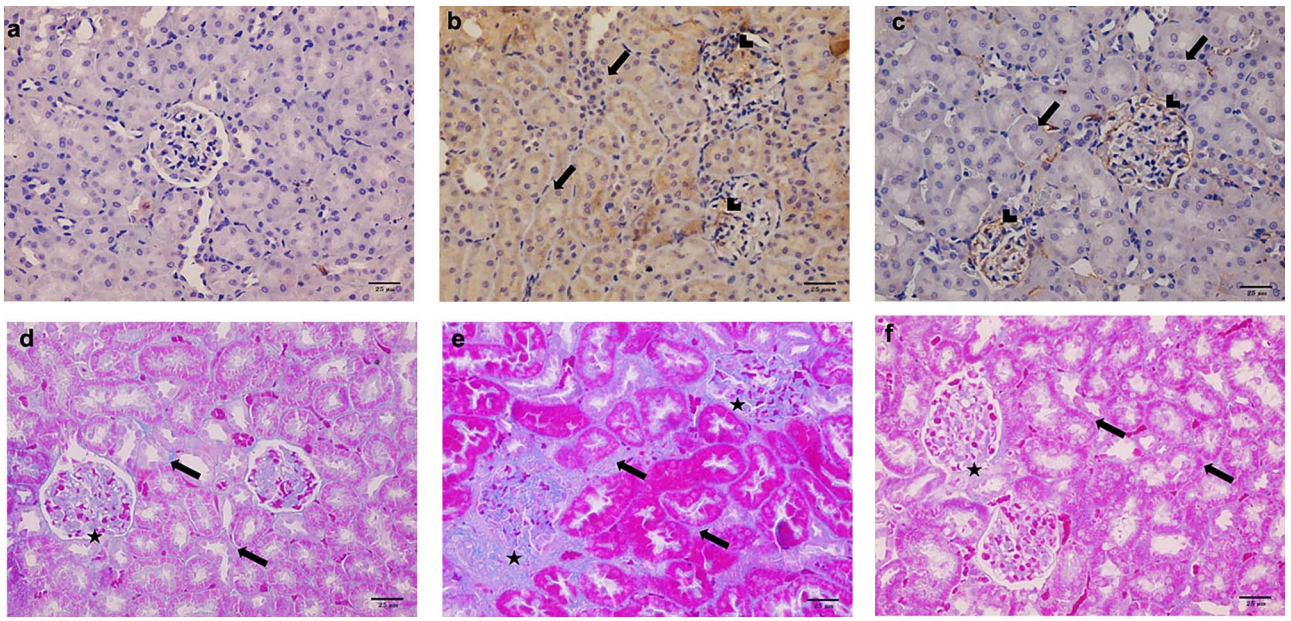

Figure 3: (**a**) The renal cortex of a control rat showing negative immunoreaction for TGF-β1. (**b**) The renal cortex of a rat from the CDDP group showing a strong positive cytoplasmic immunoreaction for TGF-β1 in renal tubules (arrows) and glomeruli (arrowheads). (**c**) The renal cortex of a rat from the CDDP + LCAR group showing a slightly positive cytoplasmic immunoreaction for GF-β1 in renal tubules (arrows) and glomeruli (arrowheads). (TGF-β1 × 400), scale bar = 25 µm. (**d**) The renal cortex of a control rat showing normal distribution of collagen fibers around glomeruli (stars) and renal tubules (arrows). (**e**) The renal cortex of a rat from CDDP group showing extensive collagen fibers deposition around glomeruli (stars) and renal tubules (arrows). (**f**) The renal cortex of a rat from the CDDP + LCAR group showing minimal collagen fibers deposition around glomeruli (stars) and around renal tubules (arrows). (Mallory's trichrome 400), scale bar = 25 µm.

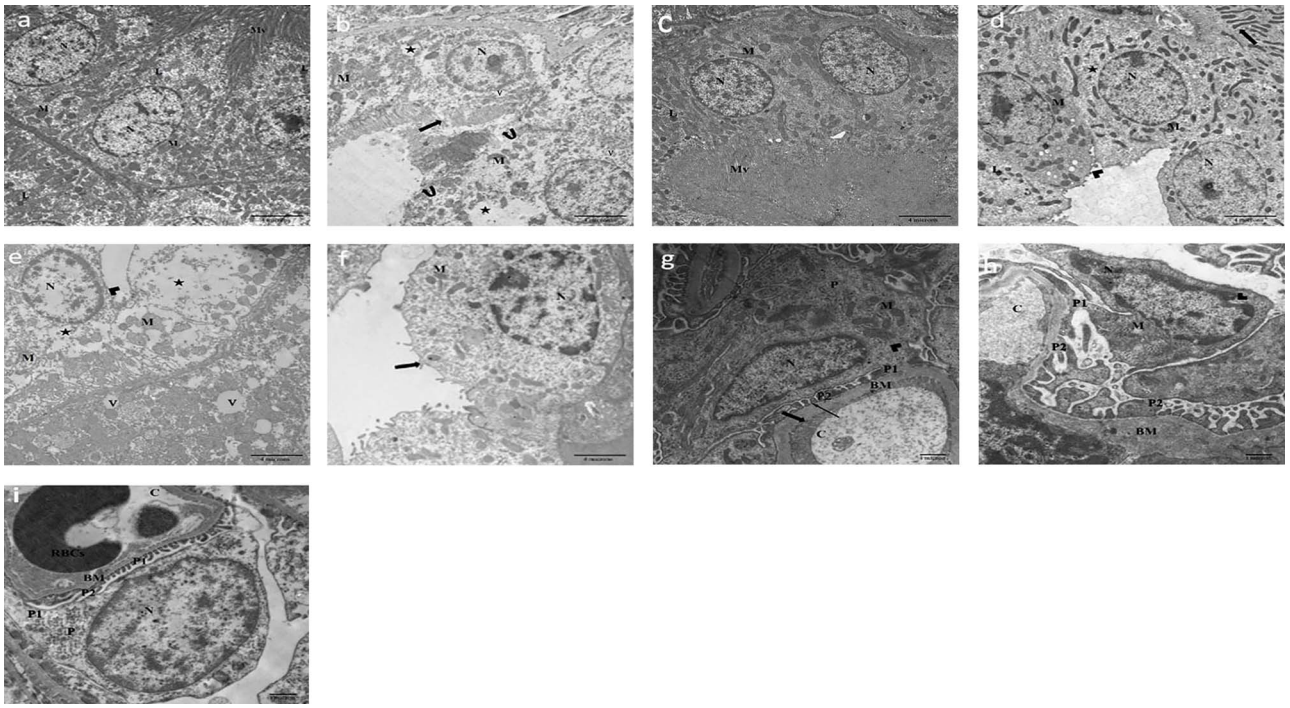

Figure 4: (**a**) Proximal convoluted tubules of a control rat showing normal tubular cells with regular euchromatic nucleus (N), continuous long apical microvilli (Mv), basally located elongated mitochondria (M) alternating with basal infoldings (arrow), and apical lysosomes (L). (**b**) Proximal convoluted tubules of a rat from CDDP group showing tubular cell with damaged apical membrane (arrow) with extrusion of cellular organelles into lumen, partial absence of apical microvilli (curved arrow) and loss of the basal infoldings. The mitochondria (M) are disorganized and degenerated. Notice, multiple cytoplasmic vacuoles (V), localized areas of rarefied cytoplasm (stars), and nucleus with extended chromatin (N). (**c**) Proximal convoluted tubules of a rat from the CDDP + LCAR group showing almost normal tubular cells with regular euchromatic nucleus and extended chromatin (N). The apical microvilli (Mv) appear long and closely packed. Mitochondria (M) appear elongated, with intact apical lysosomes (L). (**d**) Distal convoluted tubules of a rat from control group showing normal tubular cells provided with short apical microvilli (arrowhead) and rounded euchromatic nucleus (N), intact basal infoldings (arrow) with alternating elongated mitochondria (M) and lysosomes (L). (**e**) Distal convoluted tubules of a rat from CDDP group showing injured tubular cells with loss of the apical microvilli (arrowhead), markedly rarefied cytoplasm (stars), and electron lucent nucleus with dispersed chromatin (N). Cytoplasmic vacuoles (V), disrupted basal infoldings, and degenerated swollen mitochondria (M) are seen. (**f**) Distal convoluted tubules of a rat from CDDP + LCAR group showing almost normal tubular cells with irregular nucleus (N), normal elongated mitochondria (M) and short apical microvilli (arrow). (**g**) Renal glomeruli of a control rat showing a glomerular capillary (C) lined by fenestrated endothelium (thick arrow) resting on a basement membrane (BM). A podocyte (P) is seen with euchromatic nucleus (N), multiple mitochondria (M), primary thick process (P1), multiple thin secondary processes (P2) resting on the glomerular BM with filtration slits (thin arrow) in-between. (**h**) Renal glomeruli of a rat from the CDDP group showing abnormal ultrastructure of the renal glomerulus. They show irregular focal thickening of the glomerular basement membrane (BM), the secondary processes (P2) appear broad and thickened with almost fusion and subsequent obliteration of the filtration slits (thin arrow). The podocyte nucleus (N) appears indented (arrowhead) with marginally condensed chromatin. (**i**) Renal glomeruli of a rat from CDDP + LCAR group showing normal podocyte (P) with euchromatic nucleus (N), normal thick primary process (P1) and multiple thin secondary processes (P2) resting on BM of glomerular capillary (C) that contains red blood cells (RBCs), scale bar = 4 μm.

LCAR supplementation improved CDDP-induced deteriorated kidney function biomarkers in rats

Mean serum urea and creatinine significantly increased in the CDDP group than control, LCAR, and CDDP + LCAR groups ($P < 0.001$, each) (Fig. 5a).

LCAR supplementation restored renal oxidant/antioxidant balance, dampened renal inflammation and antagonized caspase 3-mediated apoptotic cell death following CDDP administration in rats

We found that CDDP treatment significantly increased mean renal levels of MDA, the inflammatory TNF-α and caspase-3 activity compared with control rats ($P < 0.001$, each), LCAR supplementation ($P < 0.001$, each), and CDDP + LCAR groups ($P = 0.036$, $P = 0.011$ and $P < 0.001$, respectively). Also, CDDP treatment significantly decreased mean renal CAT activity and the anti-inflammatory IL-10 level compared with control rats ($P < 0.001$, each), LCAR ($P < 0.001$, each) and CDDP + LCAR groups ($P < 0.001$ and $P = 0.027$, respectively) (Table 2).

LCAR supplementation down-regulated renal cytoskeleton proteins encoding genes following CDDP administration in rats

CDDP significantly up-regulated the mean expression levels of Vim, Nes, and Cx43 compared with the control group ($P < 0.001$, each) and LCAR-supplemented group ($P < 0.001$, each). LCAR supplementation significantly down-regulated their mean expression levels following CDDP treatment ($P < 0.001$ each) (Fig. 5b).

Discussion

Our results suggested the curative role of LCAR supplementation in a rat model of CDDP-induced kidney injury. Generally, CDDP-induced nephrotoxicity is widely accepted as a model for AKI [39, 40]. The nephrotoxicity of CDDP might be mediated by the generation of free radicals in response to CDDP treatment leading to oxidant–antioxidant imbalance and renal tissue injury [12, 40]. In this study, CDDP administration induced marked renal histological and ultrastructural degenerative changes in rats. These findings were consistent with a study of Ahmed and Fouad

Table 2: Effects of LCAR on renal biomarkers of oxidative stress, inflammation, and apoptosis pathway in CDDP-induced kidney injury in rats

Parameter	Groups			
	Control	LCAR	CDDP	CDDP + LCAR
MDA (nmol/g)	$19.5 \pm 5.1^{\dagger}$	$20.1 \pm 3.2^{\dagger}$	$37.5 \pm 6.7^{\ddagger}$	$30.0 \pm 1.2^{\S}$
CAT (U/g)	$43.8 \pm 3.6^{\dagger}$	$45.7 \pm 4.6^{\dagger}$	$19.4 \pm 5.8^{\ddagger}$	$34.6 \pm 6.9^{\S}$
TNF-α (pg/100 µg protein)	$8.9 \pm 1.9^{\dagger}$	$9.5 \pm 2.8^{\dagger}$	$22.5 \pm 3.0^{\ddagger}$	$15.7 \pm 4.9^{\S}$
IL-10 (pg/100 µg protein)	$9.6 \pm 2.5^{\dagger}$	$10.4 \pm 1.9^{\dagger}$	$4.6 \pm 0.7^{\ddagger}$	$6.4 \pm 1.5^{\S}$
Caspase-3 (ng/g)	$5.4 \pm 1.4^{\dagger}$	$5.1 \pm 1.7^{\dagger}$	$15.6 \pm 3.6^{\ddagger}$	$8.6 \pm 0.9^{\S}$

All values are expressed as mean ± SD, $n = 10$, means in a row without a common symbol significantly differ ($P < 0.05$) by a one-way ANOVA followed by post hoc Tukey's multiple comparisons test or Welch's one-way ANOVA followed by post hoc Tamhane's T2 multiple comparisons test. Abbreviations: MDA, Malondialdehyde; CAT, Catalase; TNF-α, Tumor necrosis factor-α; IL-10, Interleukin-10

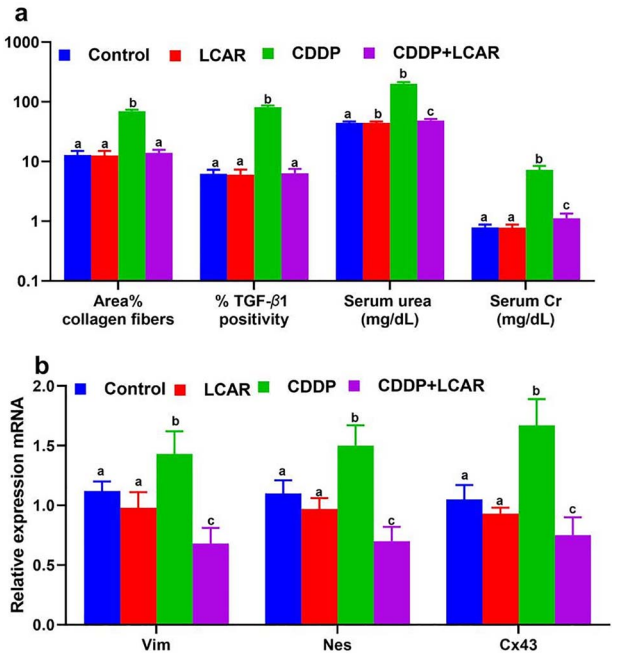

Figure 5: (**a**) Effect of LCAR on area percent of collagen fibers deposition, TGF-β1 and kidney function biomarkers in CDDP-induced kidney injury in rats. Bars not sharing the common superscript letters differ significantly at $P < 0.05$. (**b**) Effects of LCAR on the relative mRNA expression levels of Vim, Nes, and Cx43 in renal tissues. Bars not sharing the common superscript letters differ significantly at $P < 0.05$

[41] that reported marked ultrastructural damage in the kidney of CDDP-treated rats.

A renal mitochondrial injury is an early event caused by CDDP [42]. In our study, CDDP provoked mitochondrial structural impairment as documented by TEM. Mukhopadhyay [43] reported that the most protuberant ultrastructural finding of CDDP-induced renal impairment was mitochondrial swelling with disruption of cristae practically in all tubular cells.

TGF-β1 is a proinflammatory and profibrotic cytokine that can potentiate the inflammatory process elicited in the renal tissue, after initial toxic insult [44, 45]. Our study showed excess deposition of collagen fibers in renal tissues following CDDP. This massive deposition of collagen fibers could be illustrated by the overexpression of TGF-β1, with subsequent collagen production. Several studies concluded similar findings [46].

In the present study, CDDP-intoxicated rats showed up-regulation in the Vim, Nes, and Cx43 expression levels, mirroring the altered podocytes function secondary to their injury as presented by TEM [47]. In corroboration, a study of Francescato and coworkers [48] showed overexpression of Vim immunostaining in the tubulointerstitial area of renal tissues. Vim overexpression is a marker of renal tubular cell regeneration, indicative of recent injury [49, 50]. Up-regulation of Nes provides more mechanical stability to the cells and enables the podocytes to undergo morphological changes that influence the glomerular capillary wall with the subsequent decline of the renal function [51]. Cx43 is a critical modulator of podocyte function in response to CDDP-induced renal injury. Besides, Cx43 has recently been incriminated in fibrosis and inflammation cascade. Blunting Cx43 could mitigate renal damage and maintain its function [52].

We found that LCAR supplementation for 15 successive days improved the renal histological, ultrastructural and biochemical alterations elicited by CDDP. The biological functions of LCAR extend beyond its role in the transport of fatty acids into the mitochondrial matrix. Plenty of previous studies explored the efficacy of LCAR against different xenobiotics induced-organ toxicities [53–55].

We found that LCAR strongly alleviated mitochondrial dysfunction in rats exposed to CDDP as seen by TEM. Similar findings were reported by Chang *et al.* [42].

LCAR mitigated inflammation and reduced TGF-β1 immunoexpression with subsequent minimal collagen accumulation in the renal interstitium. In agreement, Rabie and coworkers [56] showed that LCAR reduced renal content of pro-inflammatory TNF-α and myeloperoxidase activity in a rat model of renal ischemia/reperfusion injury.

The down-regulation of Vim, Nes, and Cx43 expression levels following LCAR supplementation in CDDP-treated rats could be explained by its anti-inflammatory and antiapoptotic potentials [57–59]. These cytoskeleton supporting proteins are not just primarily structural proteins. They are implicated in many biological processes such as cell motility and migration, cell signaling and division, tissue regeneration, in addition to inflammation and apoptosis [18, 52].

Conclusions

LCAR supplementation reversed the negative effects of CDDP in a rat model of CDDP-induced kidney injury. This will open novel perspectives for the utilization of LCAR in the treatment of renal diseases associated with CDDP use. Furthermore, unique therapies targeting Vim, Nes, and Cx43 blunting may be practical options for effectively inhibiting the renal toxicity in patients receiving CDDP.

Conflict of interest statement

The authors have no conflicts of interests.

Funding

The authors confirm they did not receive any funding to do this work.

References

1. Gold JM, Raja A. *Cisplatin (Cisplatinum)*. Treasure Island (FL): StatPearls Publishing, 2020.
2. WHO. *World Health Organization model list of essential medicines, 21st list*. Geneva, Switzerland: World Health Organization, 2019. https://apps.who.int/iris/bitstream/handle/10665/325771/WHO-MVP-EMP-IAU-2019.06-eng.pdf?ua=1.
3. Dasari S, Bernard Tchounwou P. Cisplatin in cancer therapy: molecular mechanisms of action. *Eur J Pharmacol* 2014;**740**:364–78. doi: 10.1016/j.ejphar.2014.07.025.
4. Chawla LS, Eggers PW, Star RA et al. Acute kidney injury and chronic kidney disease as interconnected syndromes. *N Engl J Med* 2014;**371**:58–66. doi: 10.1056/NEJMra1214243.
5. Maass C, Sorensen NB, Himmelfarb J et al. Translational assessment of drug-induced proximal tubule injury using a kidney microphysiological system. *CPT Pharmacometrics Syst Pharmacol* 2019;**8**:316–25. doi: 10.1002/psp4.12400.
6. Volarevic V, Djokovic B, Jankovic MG et al. Molecular mechanisms of cisplatin-induced nephrotoxicity: a balance on the knife edge between renoprotection and tumor toxicity. *J Biomed Sci* 2019;**26**:25. doi: 10.1186/s12929-019-0518-9.
7. Qu X, Gao H, Tao L et al. Autophagy inhibition-enhanced assembly of the NLRP3 inflammasome is associated with cisplatin-induced acute injury to the liver and kidneys in rats. *J Biochem Mol Toxicol* 2019;**33**:e22208. doi: 10.1002/jbt.22228.
8. Oh GS, Kim HJ, Shen A et al. Cisplatin-induced kidney dysfunction and perspectives on improving treatment strategies. *Electrolyte Blood Press* 2014;**12**:55–65. doi: 10.5049/EBP.2014.12.2.55.
9. Ozkok A, Edelstein CL. Pathophysiology of cisplatin-induced acute kidney injury. *Biomed Res Int* 2014;**2014**:967826. doi: 10.1155/2014/967826.
10. Lebedeva MA, Eaton JS, Shadel GS. Loss of p53 causes mitochondrial DNA depletion and altered mitochondrial reactive oxygen species homeostasis. *Biochim Biophys Acta* 2009;**1787**:328–34. doi: 10.1016/j.bbabio.2009.01.004.
11. Zhu S, Pabla N, Tang C et al. DNA damage response in cisplatin-induced nephrotoxicity. *Arch Toxicol* 2015;**89**:2197–205. doi: 10.1007/s00204-015-1633-3.
12. Hakiminia B, Goudarzi A, Moghaddas A. Has vitamin E any shreds of evidence in cisplatin-induced toxicity. *J Biochem Mol Toxicol* 2019;**33**:e22349. doi: 10.1002/jbt.22349.
13. Vaz FM, Wanders RJA. Carnitine biosynthesis in mammals. *Biochem J* 2002;**361**:417–29. doi: 10.1042/0264-6021:3610417.
14. Pekala J, Patkowska-Sokola B, Bodkowski R et al. L-carnitine—metabolic functions and meaning in humans life. *Curr Drug Metab* 2011;**12**:667–78. doi: 10.2174/138920011796504536.
15. Sayed-Ahmed MM, Shaarawy S, Shouman SA et al. Reversal of doxorubicin-induced cardiac metabolic damage by L-carnitine. *Pharmacol Res* 1999;**39**:289–95. doi: 10.1006/phrs.1998.0438.
16. Schepers AV, Lorenz C, Köster S. Tuning intermediate filament mechanics by variation of pH and ion charges. *Nanoscale* 2020;**12**:15236–45. doi: 10.1039/D0NR02778B.
17. Forsting J, Kraxner J, Witt H et al. Vimentin intermediate filaments undergo irreversible conformational changes during cyclic loading. *Nano Lett* 2019;**19**:7349–56. doi: 10.1021/acs.nanolett.9b02972.
18. Cheng F, Eriksson JE. Intermediate filaments and the regulation of cell motility during regeneration and wound healing. *Cold Spring Harb Perspect Biol* 2017;**9**:a022046. doi: 10.1101/cshperspect.a022046.
19. Eriksson JE, Dechat T, Grin B et al. Introducing intermediate filaments: from discovery to disease. *J Clin Invest* 2009;**119**:1763–71. doi: 10.1172/JCI38339.
20. Eladl M, Elsaed W, Atef H et al. Ultrastructural changes and nestin expression accompanying compensatory renal growth after unilateral nephrectomy in adult rats. *Int J Nephrol Renovasc Dis* 2017;**10**:61–76. doi: 10.2147/IJNRD.S121473.
21. Lai Y, Liang X, Zhong F et al. Allicin attenuates calcium oxalate crystal deposition in the rat kidney by regulating gap junction function. *J Cell Physiol* 2019;**234**:9640–51. doi: 10.1002/jcp.27651.
22. Hanner F, Sorensen CM, Holstein-Rathlou N-H et al. Connexins and the kidney. *Am J Physiol Integr Comp Physiol* 2010;**298**:R1143–55. doi: 10.1152/ajpregu.00808.2009.
23. Sawai K, Mukoyama M, Mori K et al. Redistribution of connexin 43 expression in glomerular podocytes predicts poor renal prognosis in patients with type 2 diabetes and overt nephropathy. *Nephrol Dial Transplant* 2006;**21**:2472–7. doi: 10.1093/ndt/gfl260.
24. Nagata M. Podocyte injury and its consequences. *Kidney Int* 2016;**89**:1221–30. doi: 10.1016/j.kint.2016.01.012.
25. Welsh GI, Saleem MA. The podocyte cytoskeleton—key to a functioning glomerulus in health and disease. *Nat Rev Nephrol* 2012;**8**:14–21. doi: 10.1038/nrneph.2011.151.
26. Kamel KM, Abd El-Raouf OM, Metwally SA et al. Hesperidin and Rutin, antioxidant citrus flavonoids, attenuate cisplatin-induced nephrotoxicity in rats. *J Biochem Mol Toxicol* 2014;**28**:312–9. doi: 10.1002/jbt.21567.
27. Naghizadeh B, Mansouri SMT, Mashhadian NV. Crocin attenuates cisplatin-induced renal oxidative stress in rats. *Food Chem Toxicol* 2010;**48**:2650–5. doi: 10.1016/j.fct.2010.06.035.
28. Naghizadeh B, Boroushaki M, Vahdati M et al. Protective effects of crocin against cisplatin-induced acute renal failure and oxidative stress in rats. *Iran Biomed J* 2008;**12**:93–100.
29. Graziano F, Bisonni R, Catalano V et al. Potential role of levocarnitine supplementation for the treatment of chemotherapy-induced fatigue in non-anaemic cancer patients. *Br J Cancer* 2002;**86**:1854–7. doi: 10.1038/sj.bjc.6600413.
30. Gramignano G, Lusso MR, Madeddu C et al. Efficacy of L-carnitine administration on fatigue, nutritional status, oxidative stress, and related quality of life in 12 advanced cancer patients undergoing anticancer therapy. *Nutrition* 2006;**22**:136–45. doi: 10.1016/j.nut.2005.06.003.
31. Kraft M, Kraft K, Gärtner S et al. L-carnitine-supplementation in advanced pancreatic cancer (CARPAN)–a randomized multicentre trial. *Nutr J* 2012;**11**:52. doi: 10.1186/1475-2891-11-52.
32. Reagan-Shaw S, Nihal M, Ahmad N. Dose translation from animal to human studies revisited. *FASEB J* 2008;**22**:659–61. doi: 10.1096/fj.07-9574LSF.
33. Şehirli AÖ. A simple practice guide for dose conversion between animals and human. *J Basic Clin Pharm* 2016;**7**:27–31. doi: 10.4103/0976-0105.177703.
34. Leal Filho MB, Morandin RC, de Almeida AR et al. Hemodynamic parameters and neurogenic pulmonary edema

following spinal cord injury: an experimental model. *Arq Neuropsiquiatr* 2005;**63**:990–6 S0004-282X2005000600016.
35. Bancroft JD, Layton C. The hematoxylin and eosin. In: Suvarna SK, Layton C, Bancroft JD (eds). *Bancroft's Theory and Practice of Histological Techniques*, 8th edn. Philadelphia: Elsevier, 2019, 126–38.
36. Bancroft JD, Layton C. Connective tissue and other mesenchymal tissues with their stains. In: Suvarna SK, Layton C, Bancroft J (eds). *Bancroft's Theory and Practice of Histological Techniques*, 8th edn. Philadelphia: Elsevier, 2019, 153–75.
37. Kiernan JA. *Histological and histochemical methods. Theory and practice*, 5th edn. Banbury, UK: Scion Publishing Ltd, 2015.
38. Woods AE, Stirling JW. Transmission electron microscopy. In: Suvarna SK, Layton C, Bancroft J (eds). *Bancroft's Theory and Practice of Histological Techniques*, 8th edn. Philadelphia: Elsevier, 2019, 434–75.
39. Shi M, McMillan KL, Wu J et al. Cisplatin nephrotoxicity as a model of chronic kidney disease. *Lab Invest* 2018;**98**:1105–21. doi: 10.1038/s41374-018-0063-2.
40. Tomar A, Kaushik S, Khan SI et al. The dietary isoflavone daidzein mitigates oxidative stress, apoptosis, and inflammation in CDDP-induced kidney injury in rats: impact of the MAPK signaling pathway. *J Biochem Mol Toxicol* 2020;**34**:e22431. doi: 10.1002/jbt.22431.
41. Ahmed SM, Fouad FE. Possible protective effect of platelet-rich plasma on a model of cisplatin-induced nephrotoxicity in rats: a light and transmission electron microscopic study. *J Cell Physiol* 2019;**234**:10470–80. doi: 10.1002/jcp.27706.
42. Chang B, Nishikawa M, Sato E et al. L-carnitine inhibits cisplatin-induced injury of the kidney and small intestine. *Arch Biochem Biophys* 2002;**405**:55–64. doi: 10.1016/S0003-9861(02)00342-9.
43. Mukhopadhyay P, Horváth B, Zsengellér Z et al. Mitochondrial-targeted antioxidants represent a promising approach for prevention of cisplatin-induced nephropathy. *Free Radic Biol Med* 2012;**52**:497–506. doi: 10.1016/j.freeradbiomed.2011.11.001.
44. Vega G, Alarcón S, San Martín R. The cellular and signalling alterations conducted by TGF-β contributing to renal fibrosis. *Cytokine* 2016;**88**:115–25. doi: 10.1016/j.cyto.2016.08.019.
45. Sisto M, Lorusso L, Ingravallo G et al. The TGF-β1 signaling sathway as an attractive target in the fibrosis pathogenesis of Sjögren's syndrome. *Mediators Inflamm* 2018;**2018**:1965935. doi: 10.1155/2018/1965935.
46. Ali DA, Abdeen AM, Ismail MF et al. Histological, ultrastructural and immunohistochemical studies on the protective effect of ginger extract against cisplatin-induced nephrotoxicity in male rats. *Toxicol Ind Health* 2015;**31**:869–80. doi: 10.1177/0748233713483198.
47. Wang W, Ding X-Q, Gu T-T et al. Pterostilbene and allopurinol reduce fructose-induced podocyte oxidative stress and inflammation via micro RNA-377. *Free Radic Biol Med* 2015;**83**:214–26. doi: 10.1016/j.freeradbiomed.2015.02.029.
48. Francescato HDC, Coimbra TM, Costa RS et al. Protective effect of quercetin on the evolution of cisplatin-induced acute tubular necrosis. *Kidney Blood Press Res* 2004;**27**:148–58. doi: 10.1159/000078309.
49. Vansthertem D, Gossiaux A, Declèves A-E et al. Expression of nestin, vimentin, and NCAM by renal interstitial cells after ischemic tubular injury. *J Biomed Biotechnol* 2010;**2010**:1–10. doi: 10.1155/2010/193259.
50. Menon S. Acute kidney injury in nephrotic syndrome. *Front Pediatr* 2019;**6**:428. doi: 10.3389/fped.2018.00428.
51. Zhang W, Zhang L, Chen Y-X et al. Identification of nestin as a urinary biomarker for acute kidney injury. *Am J Nephrol* 2014;**39**:110–21. doi: 10.1159/000358260.
52. Prakoura N, Kavvadas P, Chadjichristos CE. Connexin 43: a new therapeutic target against chronic kidney disease. *Cell Physiol Biochem* 2018;**49**:985–5. doi: 10.1159/000493230.
53. Yurut-Caloglu V, Caloglu M, Deniz-Yalta T et al. Radiation-induced acute kidney toxicity: protective effect of L-carnitine versus amifostine. *Int J Radiat Res* 2015;**13**:317.
54. Aziz M, Abd El Fattah MA, Ahmed KA et al. Protective effects of Olmesartan and L-carnitine on doxorubicin-induced cardiotoxicity in rats. *Can J Physiol Pharmacol* 2019;**98**:183–93.
55. Hejazy M, Najafi D. Renal protective effects of L-carnitine on lead-induced nephropathy in Wistar rats. *Int J Med Toxicol Forensic Med* 2018;**8**:89–94.
56. Rabie MA, Zaki HF, Bahgat AK et al. Angiotensin antagonists and renal ischemia/reperfusion: possible modulation by L-carnitine. *Bull Fac Pharmacy, Cairo Univ* 2012;**50**:7–16. doi: 10.1016/j.bfopcu.2011.12.002.
57. Zhu X, Sato EF, Wang Y et al. Acetyl-L-carnitine suppresses apoptosis of thioredoxin 2-deficient DT40 cells. *Arch Biochem Biophys* 2008;**478**:154–60. doi: 10.1016/j.abb.2008.07.024.
58. Di Cesare Mannelli L, Ghelardini C, Calvani M et al. Protective effect of acetyl-L-carnitine on the apoptotic pathway of peripheral neuropathy. *Eur J Neurosci* 2007;**26**:820–7. doi: 10.1111/j.1460-9568.2007.05722.x.
59. Yürekli Y, Ünak P, Yenisey Ç et al. L-carnitine protection against cisplatin nephrotoxicity in rats: comparison with amifostin using quantitative renal Tc 99m DMSA uptake. *Mol Imaging Radionucl Ther* 2011;**20**:1–6. doi: 10.4274/MIRT.20.01.